THEMATIC SECTION: 7TH WORLD CONGRESS ON INTEGRATED COMPUTATIONAL MATERIALS ENGINEERING

Process–Structure–Property Simulation Approach to the Estimation of Tensile Anisotropy in 3D Printed Meta-stable β Titanium Alloy

Luis M. Reig Buades[1] · Martin P. Persson[1]

Abstract

Developing accurate process–structure–property models for metal additive manufacturing is crucial due to the numerous process parameters, extended build times, and high material costs which make it impractical to rely solely on an experimental trial and error approach when optimizing the process. In this work, a multiscale digital approach to estimate tensile anisotropy along selective laser melted titanium meta-stable β alloys is presented. The approach uses a component scale thermal FEA model of the process to calculate temperature, a meso-scale phase field model to calculate microstructure evolution, and a microscale crystal plasticity model to calculate the effect of texture on the tensile properties in different directions. The model has predicted isotropic yield strength for this material, which could guide designers to choose orientations freely. However, anisotropy in hardening behavior could be expected but is caused by porosity and cracking, which are not considered in the presented models. We believe the presented approach, which relies solely on easy to use commercial simulation tools, lays a good foundation for the development of process–structure–property models to optimize process parameters. The modeling approach should be applicable to other mechanical properties and materials with appropriate considerations.

Keywords Process–structure–property–performance · Additive manufacturing · FEA · Phase field model · Crystal plasticity

Introduction

Material scientists and manufacturing engineers work on studying the process–structure–property–performance (PSPP) relations of materials and components. Process refers to the different methods in creating a given object, structure means the underlying morphologies and constituents of the object, property refers to the attributes of the object in regards to performing a given task and performance refers to the degree of satisfaction to which the object will serve its purpose. Process–structure–property–performance relations are intricately interconnected and must be well understood in order to optimize a component and its manufacturing process. Let us look at the case of an additively manufactured component. The process (Additive Manufacturing) has many variables to optimize (laser power, path, speed, size, layer thickness, etc.), which will affect the structure (grain size, segregation, phase fraction, etc.), which will affect the properties (Young's modulus, yield strength, anisotropy, ductility, etc.), which will in the end determine the component's performance. Furthermore, all of these relations will be altered by the geometry of the component and the alloy chosen.

This shows that trying to optimize a component with a designer performing elastic simulations on different geometries with constant and homogeneous mechanical properties limits significantly the degree to which the component can be optimized. Furthermore, it can even produce unrealistic performance estimations for cases like additive manufacturing, where the microstructure of the material can be heterogeneously distributed or anisotropic and therefore its mechanical properties [1, 2].

The role of Integrated Computational Material Engineering (ICME) is to integrate geometry, material selection and

---

Luis M. Reig Buades and Martin P. Persson have equally contributed to this work.

✉ Martin P. Persson
Martin.Persson@3ds.com

Luis M. Reig Buades
luis.reig97@gmail.com

[1] BIOVIA, Dassault Systemes, 22 Cambridge Science Park, Milton Road, Cambridge CB4 0FJ, UK

manufacturing parameters in the design of a component and to exploit the whole design window through simulations. From a computer-aided-engineering (CAE) software development perspective, the ultimate goal would be to take the user requirements for a structural component (geometrical constraints and loads) and be able to optimize the component's geometry, manufacturing parameters and alloy composition for the component through a combination of many multiscale and topology simulations together with surrogate machine learning models. Unfortunately, this end goal is still remote due to the underdevelopment and computational expense of the multiscale multi-physics simulations needed for this. Nonetheless, ICME models able to predict performance of a given component from its manufacturing process are starting to appear and get attention. Yan et. al. developed a process–structure–property model coupling CFD, cellular automaton and full-field micromechanics to predict fatigue life [3]. Turner et. al. are using a similar approach to estimate the heterogeneous mechanical properties of a component during printing and obtain accurate residual stress predictions [4]. Motaman et. al. also used multiscale simulations to calculate tensile properties, but they also included CALPHAD and first principles simulations to optimize the alloy composition [5]. These show that it is certainly feasible to develop PSPP models of AM processes. However, they have all been performed by large groups of experienced university or national-lab researchers with deep computational modeling knowledge mostly using in-house software libraries. If these models are to be developed and used by manufacturing engineers, with a more product-focused approach, more accessible software tools for the different simulations in the multiscale PSPP chains are needed.

In this work, a digital approach to estimating the tensile anisotropy of additively manufactured alloys is proposed using commercial tools that do not require deep software engineering knowledge. As a proof of concept, we will be focusing on laser powder bed fusion (LPBF) of Ti-5553. To the knowledge of the authors, no process–structure–property models have been presented for anisotropy prediction in powder bed fusion of Ti-5553. However, this modeling approach should be applicable to other alloys with due consideration. In the approach presented, BIOVIA's phase field simulation tools are used to calculate the microstructure obtained from the manufacturing process, and they are connected with SIMULIAS's tools to close the whole process-property-structure-performance circle.

Firstly, Abaqus is used for macro-scale FEA models of the manufacturing process, capturing the effect of manufacturing parameters like laser speed and power on the temperatures the component experiences. The temperature histories are extracted and used as inputs for the phase field simulations. Phase field simulations produce representative volume elements (RVEs) which are then meshed and imported back into Abaqus. By applying a load with periodic boundary conditions on the obtained RVE, homogenized mechanical properties of a given microstructure can be obtained. A schematic of the proposed PSPP approach is seen in Fig. 1, which also shows how the calculated mechanical properties from this approach could be used in a mechanical FEA model to assess the structural performance of the final component, coupling the design of a component's geometry and its manufacturing process.

Methodology

Thermal FEA Model

Ti-5553 forms a fully meta-stable BCC phase during the PBF process, caused by the rapid cooling rates inherent to the process. Due to the lack of precipitation during printing of this alloy, its mesoscale morphology will be influenced mainly by the cooling rate and thermal gradients experienced while the material is solidifying. These quantities can be calculated by a thermal FEA simulation if the process is modeled adequately.

Thermal FEA models solve the heat conduction equation in arbitrary domains. By considering moving heat sources and element addition, they can be used to calculate thermal phenomena along a component during metal additive manufacturing, and have been proven to yield accurate melt-pool temperatures [6]. Abaqus additive manufacturing plug-in is used here for the thermal FEA simulation. It uses tool-path information in the form of tabular data to consider the laser as a moving heat source and layer addition by modifying the FEA domain during the simulation. Furthermore, it tracks how the domain changes along the printing to modify where convection and radiation are applied. More information about the plug-in can be found in the Abaqus user manual [7].

For this work, the printing of a 2.5 mm square column with a 20 mm height will be simulated. The thermal gradient and cooling rates during solidification at different layer heights will be extracted. These will later be used in the Phase Field model to model the solidification microstructure. Calculating them at different layers allows to assess if different heights will experience different thermal gradients or cooling rates and therefore if the structure will be heterogeneous.

The geometry of the printed column and the substrate is seen in Fig. 2. The figure also shows the mesh used. For each layer printed, a refined mesh of 60 μm side length is maintained only around the layer being printed, and it gradually coarsens in the remote regions where the thermal gradients are significantly lower. This makes it possible to model a large geometry, which would be computationally unfeasible
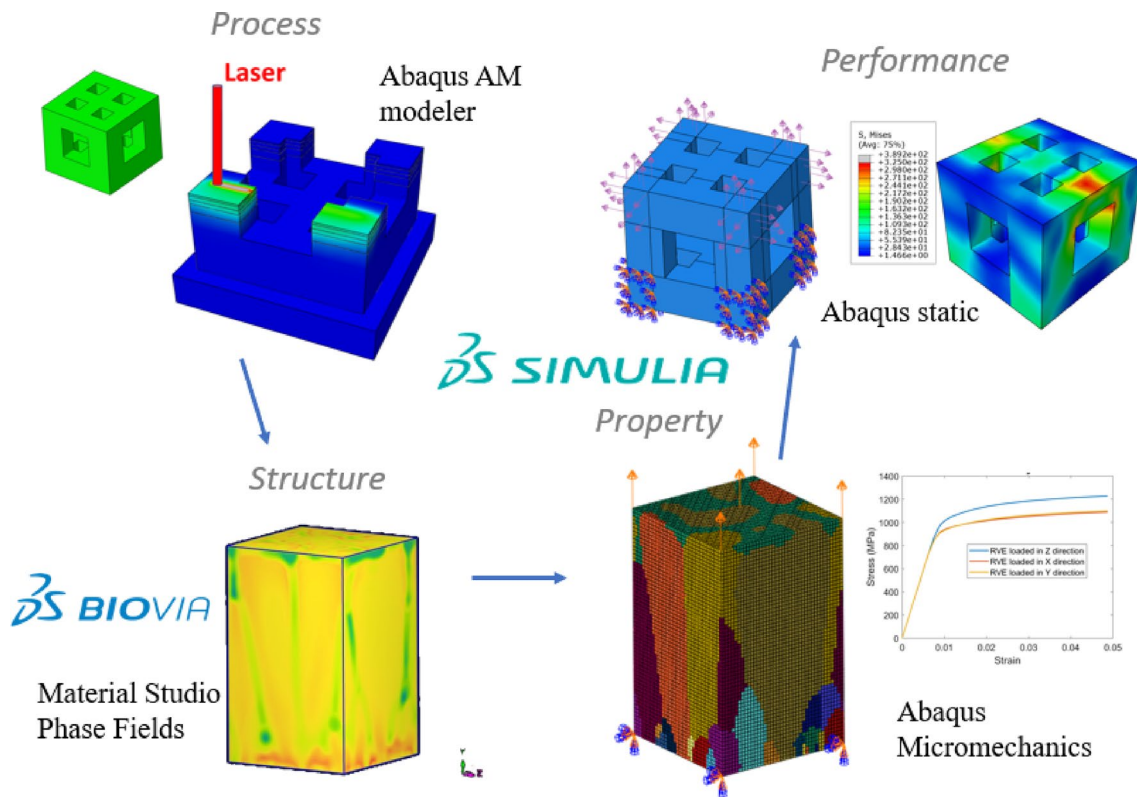
Fig. 1 Schematic of the PSPP approach presented. The AM modeler in Abaqus is used to relate geometry and process parameters to local temperature history. BIOVIA's phase field tools are used to simulate the microstructure produced by the previously obtained temperature history. Abaqus micromechanics plug-in is used to digitally test a given microstructure and obtain its anisotropic mechanical properties. Finally, Abaqus can also be used to assess the structural performance of the printed component to its design load with the previously calculated mechanical properties

Fig. 2 Mesh used in the thermal FEA model. The figure corresponds to the mesh of the last layer, showing how the printed column would look on the substrate. The layer-wise re-meshing approach used can be seen, where a fine mesh is only maintained around the layer being printed
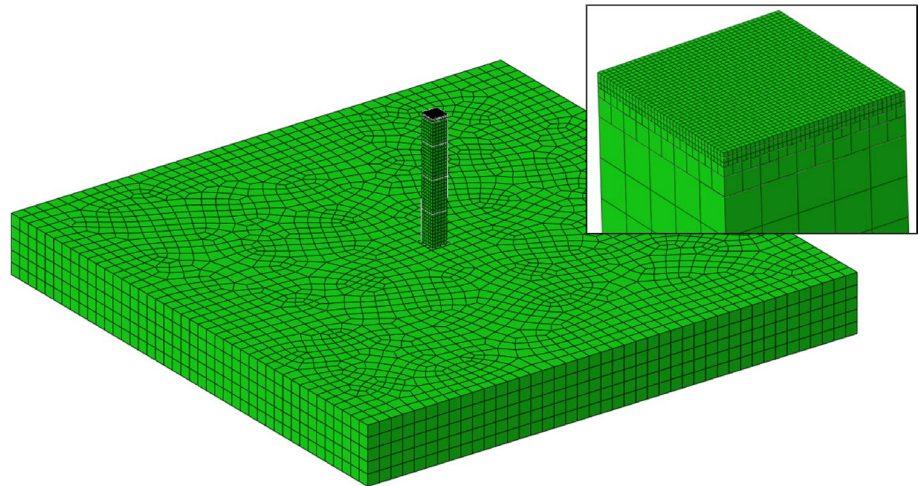
with a static mesh. Tie constraints were used to allow for the rapid mesh transition (Figs. 3, 4).

Besides the adaptive meshing strategy, the thermal FEA model used follows a similar methodology to ref. [2] to model Ti-6Al-4V, to which we refer the readers for a more detailed description of the Abaqus approach to the thermal modeling of LPBF. The temperature dependent thermal properties used here for Ti-5553 are displayed in 3. A constant density value of 4.65 g/cm³ is used. Abaqus metallurgical phase transformation framework is activated to include
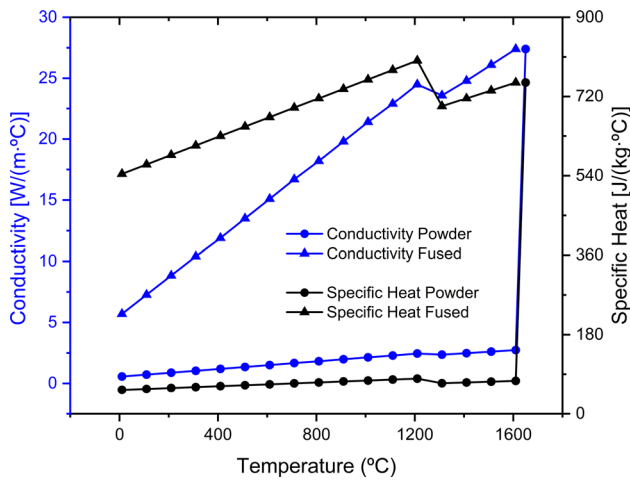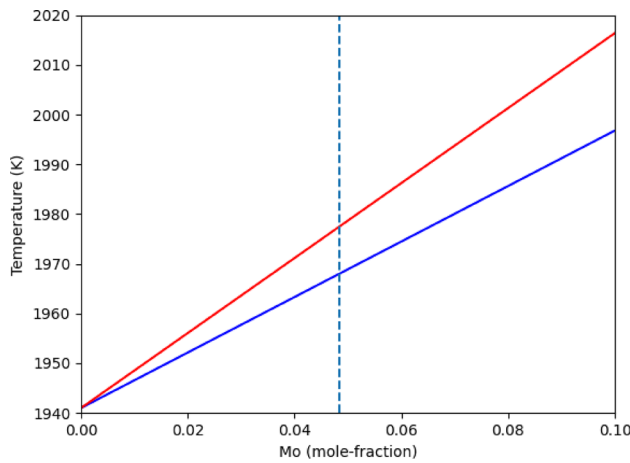
Fig. 3 Conductivity and specific heat

Fig. 4 Linearized approximation of the Ti-5553 pseudo binary phase diagram used in phase field calculations. The red line is the liquidus line between the liquid and BCC phase and the blue line is the solidus line. Initial concentration for the liquid is marked with a dashed line

an internal state variable approach that applies a lower conductivity and specific heat to the elements before they have been melted. This allows to account for the different thermal properties of the powder. Once they reach the melting temperature of 1660 °C, the thermal properties are made to match those of the solid metal. Regarding boundary conditions, convection with a coefficient of $h = 18\,W/(°C * m^2)$ and radiation with an emissivity of $\epsilon = 0.25$ to an air temperature of 26 °C are also considered. The built plate was not heated and started at the air temperature of 26 °C. This temperature value was also applied to the elements that activate during the simulation which represent powder addition.

The scanning strategy modeled consists of a simple meander hatching with a 90 ° rotation. The hatch spacing is $h = 0.12$ mm. The laser power and speed are $P = 375\,W$ and

$v = 1029$ mm/s, respectively. The layer thickness is 60 μm. The inter-layer time was 8 s. The heat addition was modeled as a volumetric heat flux with Goldak distribution with the approach from ref. [2] with a laser spot radius of $r = 75$ μm. The laser power absorption coefficient was 55%.

The temperature gradient and temperature rates are directly calculated by Abaqus and output as field or history data, if requested. Therefore, they can be obtained at the desired element and time without any intricate post-processing. For our purposes, these parameters will be extracted at different heights for different elements of the melt pool boundary, which corresponds to regions with a temperature of 1660° during cooling.

Phase Field Model of Microstructure Evolution

The temperature rate and gradient values extracted from the thermal FEA model can be used to setup a phase field model of the microstructure produced during the solidification of the melt pool. The solidification is modeled using the phase field tools available in BIOVIA's Pipeline Pilot, Materials Studio Collection [8]. The executable used by the phase field tools is based on the OpenPhase commercial library [9–11]. The setup of the model and analysis of the result is done in BIOVIA's Materials Studio tool [12]. The result from the simulations are brought back as time series data and field trajectories. The resulting RVEs are also returned in Abaqus input format transferring grain data such as crystallographic orientation and elastic properties to an Abaqus RVE model. Since the mesh used for the phase field model is finer than what is needed for the FEA models. The mesh for the Abacus RVE is re-meshed to a coarser mesh to better suite the requirement of the mechanical FEA models.

To simplify the model and to reduce the computational effort, the Ti-5553 thermodynamic data was setup as a pseudo binary linearized version of the phase diagram, see Fig. 1, in the same way as by Agius et al [13]. The pseudo binary phase diagram was generated using ThermoCalc [14]. Since the simulation only model the rapid solidification of the melt pool and not any post solidification thermal treatment, the diffusion parameters are defined as constant values (Tables 1, 2).

Table 1 Thermodynamic parameters used in the phase field simulation

Parameter	Symbol	Value
Equilibrium temperature	T_e	1977.48 K
Equilibrium concentration liquidus	$c_{l,Ti}$	0.9516 mole-fraction
Equilibrium concentration solidus	$c_{s,Ti}$	0.9346 mole-fraction
Diffusion coefficient (liquid)	D_s	5×10^{-13}
Diffusion coefficient (solid)	D_l	5×10^{-13} m²/s
Entropy Difference	ΔS_{sl}	9.633 J/K/mol

Table 2 Phase field input parameters used in the phase field simulation

Parameter	Symbol	Value
Time step	Δt	$\approx 5 \times 10^{-8}$ s (adaptive time step)
Grid spacing	Δx	5×10^{-7} m
Interface energy	σ	0.071 Jm^{-2}
Interface energy anisotropy	ϵ_σ	0.5
Interface mobility	μ_{sl}	2.46×10^{-7} m^4/Js
Interface mobility	μ_{ss}	2.46×10^{-10} m^4/Js
Interface mobility anisotropy	ϵ_μ	0.5
Initial temperature	T_s	1973 K
Temperature rate	dT/dt	-5×10^4 K/s
Temperature gradient	dT/dy	1×10^5 K/m

Table 3 Parameters used in the phenomenological crystal plasticity constitutive model for the micromechanics FEA simulation [13]

Parameter	Symbol	Value
Young's Modulus	E	85000 MPa
Poisson's ratio	v	0.35
Initial Hardening Modulus	h_0	13120 MPa
Critical Resolved Shear Stress	τ_0	300 MPa
Saturation Value of Flow Stress	τ_s	353 MPa
Slip System Interaction Constant	q	1
Reference Strain Rate	$\dot{\gamma}_0$	0.0001 s^{-1}
Rate sensitivity exponent	m	19.3 MPa

Our approach to the microstructure prediction focuses on prediction of the large scale grain structure, ignoring any fine structure such as dendrite formation. Hence, the phase field simulation is run using a relatively coarse grid. The phase field model is set up as a 60 μm tall cell with a base of 37.5×37.5 μm^2 using a 5×10^{-7} grid spacing. The bottom of the cell is initialized with 64 cubic nucleation sites with random orientation. Since the thermal model has yielded homogeneous cooling rate and thermal gradient along the build during solidification, the microstructure should be homogeneous. For this reason, a single set of thermal conditions will be modeled. For reasons of computational cost we chose a lower cooling rate and temperature gradient compared to the result from the thermal FEA model. Due to limitations in the phase field code a constant cooling rate and thermal gradient was applied. The temperature at the start of the simulation is set to 1973 K at the base of the cell and with a constant temperature gradient of 1×10^5 K/m. The system is then cooled at a rate of -5×10^4 K/s. The anisotropy coefficient of the interface energy and the interface mobility is set to 0.5, which will result in certain grain orientations being favored by the large thermal gradient in the melt pool. The interface mobility for the solid liquid interface was scaled up until the resulting micro structure came back without any liquid between grains. The system is allowed to grow until the solid phase has reached the top of the cell. The final micro structure brought back in Abaqus input format with a 2 times coarser mesh. The time evolution of the micro structure is tracked in the form of property data such as phase fractions and grain volumes. Time sequences of the micro structure field data is also brought back in the form of field trajectories.

micromechanical Simulation for Property Calculation

As previously explained, BIOVIA's Material Studio gives the option to output the obtained microstructure of the Phase Field Simulation as an Abaqus input file. This Abaqus input file contains a hexahedral mesh with a user-defined number of elements in each direction by resizing the original phase field mesh. This is useful because phase field simulations usually require a much higher discretization than mechanical FEA meshes. For the obtained microstructures, a mesh of 38x38x60 linear elements yielded adequate discretization. The generated mesh is separated in element sets for each grain, which have been assigned different material orientations corresponding to the crystallographic orientation of each grain in the phase field results. This way, the crystallographic texture and grain morphology predicted by the phase field simulation can be used in a mechanical FEA simulation to digitally test the microstructure with a desired loading scenario.

Using the Abaqus micromechanics plug-in, it is straightforward to set up digital mechanical testing of an RVE with PBCs and obtain the volume averaged stress–strain curve with the desired loading scenario. We refer the reader to the micromechanics plug-in documentation for more detailed information on the application of PBCs and the calculation of field averages [7].

Regarding the constitutive model to represent the microstructural response to a load, the widely known phenomenological crystal plasticity (CP) model has been used, initially developed by Peirce, Asaro and Needleman [15]. All slip systems directions corresponding to the BCC crystal structure have been considered. These are the $\{110\} < 111 >$, $\{211\} < 111 >$ and $\{321\} < 111 >$ directions, which produce a total of 48 slip systems being tracked by the constitutive model. The crystal plasticity parameters used are displayed in Table 3, obtained from [13]. The constitutive model was applied with the UMAT subroutine developed by Huang [16]. Since the solidified

material contained a single phase, the same constitutive model could be applied to the whole RVE, differentiating grains by element sets having different material orientations. It must be noted that the used phenomenological micromechanics CP model may not be enough to quantitatively predict a tensile strength value, but it considers the effect of texture on strength and can qualitatively yield the direction of highest strength.

By considering microstructural morphology and texture, CPFEA models of microstructural RVEs can output a lot of information about the mechanical performance of a microstructure. Some applications of CPFEA include fatigue initiation analysis [17], texture evolution [18] and even crack propagation [19]. Another important application is homogenization, which consists of extracting macroscopic bulk properties of the material by digitally testing the RVE. For this work, we will analyze the anisotropic elastic–plastic tensile properties. Since a columnar and textured microstructure is expected, the volume averaged stress–strain curves of uni-axial tension in the vertical and horizontal directions with a strain rate of 10^{-4}s^{-1} will be compared. Due to the randomness in nucleation, five different RVEs will be simulated and their stress–strain behavior will be averaged.

Results

Thermal FEA Model

Figure 5 shows the field output contours of the nodal temperature, temperature rate and temperature gradient obtained from the thermal FEA model along different views. The shown outputs correspond to the printing of the middle bead of the 10 mm height layer. The melt pool is shown by giving a gray color to all regions with a temperature above the melting point of 1660 °C in the temperature contours. With this view, it is straightforward to probe the temperature rates and gradients in the melt pool boundary using the "Probe Values" tool in Abaqus. Another way to obtain these would be to create a melt pool tracking algorithm, which is planned to be developed in future. The temperature gradient and cooling rates have been probed at the centroid of the tail and belly elements of the meltpool, which have been marked as such in Fig. 5b)

The obtained values of the temperature rate and gradients obtained at the different heights is seen in Table 4. The results show that there is not a significant change in values at the different layer heights. Although not shown
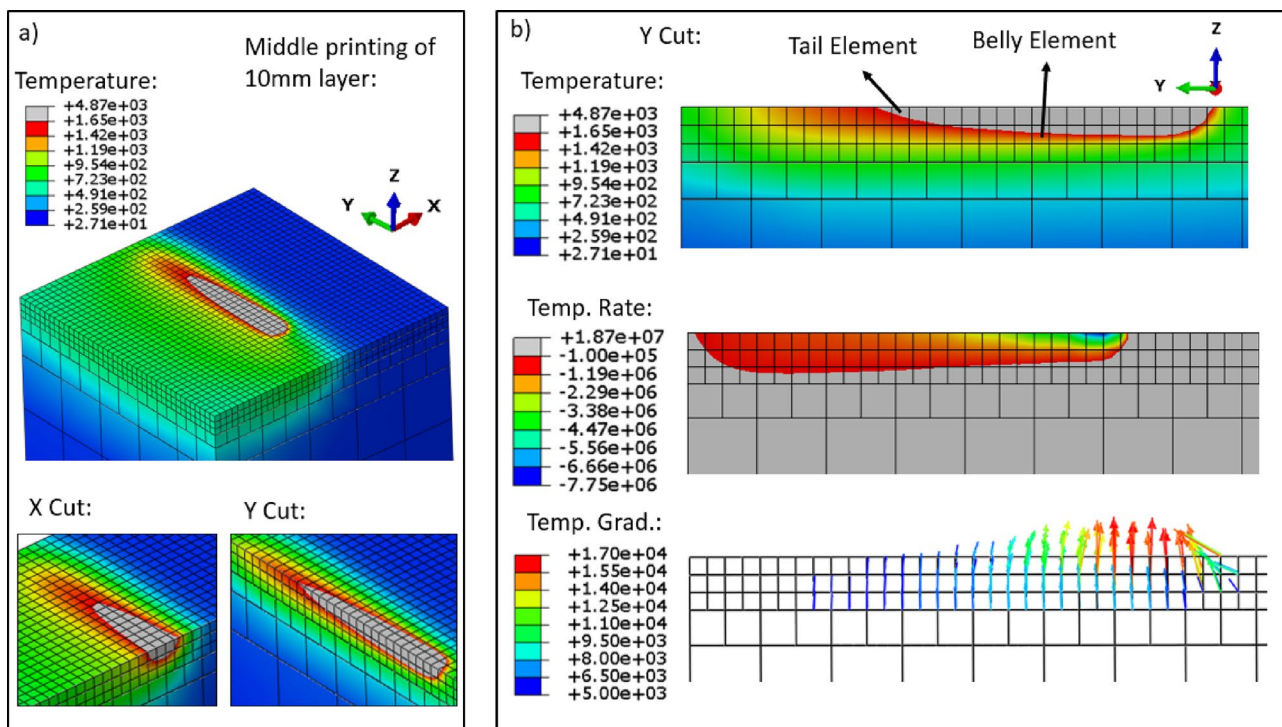
Fig. 5 Field Outputs of the thermal FEA model during printing of the 10 mm height layer. All outputs are presented at the same time increment, which corresponds to scanning the middle bead. **a** shows a 3D view of nodal temperature output together with two orthogonal cuts. All temperatures above the melting temperature of 1660 °C are shown in gray, in order to display the geometry of the melt pool. **b** shows the temperature, gradient and cooling rate, field outputs obtained in the simulation. It also shows the two elements from which the temperature rate and gradient values will be extracted for analysis

here, the melt pools obtained also had similar shapes. This means that for the process parameters used, the solidified microstructure will be similar along the printed component without significant heterogenities. This also implies that the differences in residual heating and distance from the substrate do not affect much the melt pool behavior for this material and parameters. It must be noted that these values have been compared in the center of a column, and different geometries like downskins or thin walls could induce significant differences in the melt pool behavior that have not been studied here. Nonetheless, these results can allow us to assume that the bulk properties of PBF Ti-5553 material with these process parameters will be homogeneous.

Another issue to point out is that the thermal gradients obtained in the melt pool are predominantly vertical, which is seen in Fig. 5b). This is important because in additive manufacturing the high thermal gradients can induce grains with a particular orientation to solidify faster, producing a

microstructure with a predominant crystallographic orientation. By using the obtained magnitude and direction of the thermal gradients in the phase field solidification model, it will output the final crystallographic orientations for this material and process parameters.
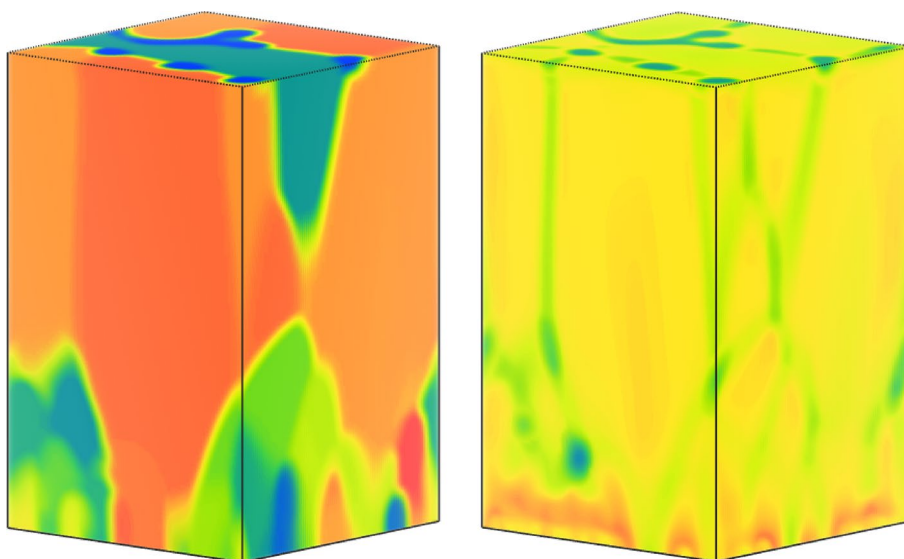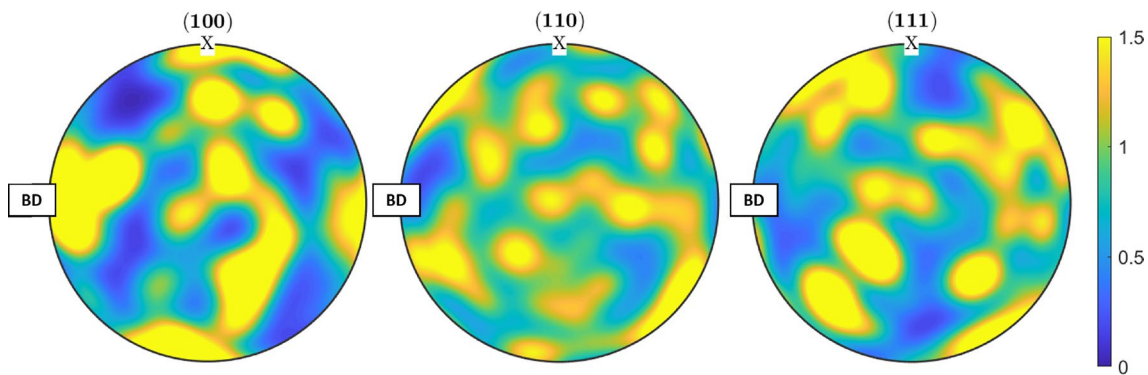
Microstructure Prediction

In order to allow statistical analysis, 5 microstructures were simulated with random initial positions and orientations for the nucleation sites. Figure 6 shows an example of the resulting microstructure and composition. The base of the cell has a large number of small equiaxed grains. While the rest of the cell is dominated by large elongated grains. These elongated grains are found to have a crystal orientation aligned with the thermal gradient. This is seen in the pole figures in Fig. 7, which shows a < 100 > fiber texture with respect to the build direction. This is an effect of the interfacial anisotropy included in the model, where as the grains continue to grow, grains with a favorable orientation relative to the thermal gradient will grow faster than the average grains and eventually dominate the upper part of the micro structure. This agrees with the experimental results in ref. [20]. However, the < 100 > fiber texture measured experimentally is more pronounced than in these simulations. This implies that the size or number of RVEs simulated might not be enough to represent an average of the microstructure. This matter requires further study, which will be performed in future work. Besides grain morphology and orientation, phase field simulations also output solute distribution. For this material, since the grains solidify with a higher concentration than the liquid, the interface between grains tends to have a lower Mo concentration than the interior.

Table 4 Cooling rate and temperature gradients of the belly and tail elements of the melt pool at different layer heights

Layer Height	Position	Cooling Rate (K/s)	Temp. Gradient (K/m)
5 mm	Tail Element	$826 * 10^3$	$4.39 * 10^6$
	Belly Element	$216 * 10^3$	$11.8 * 10^6$
10 mm	Tail Element	$823 * 10^3$	$4.36 * 10^6$
	Belly Element	$220 * 10^3$	$11.7 * 10^6$
15 mm	Tail Element	$822 * 10^3$	$4.34 * 10^6$
	Belly Element	$223 * 10^3$	$11.7 * 10^6$
20 mm	Tail Element	$822 * 10^3$	$4.34 * 10^6$
	Belly Element	$224 * 10^3$	$11.6 * 10^6$

Fig. 6 (left) Typical microstructure × 2 resulting from the phase field simulations. The bottom consists of a large number of small equiaxed grains while the upper half is dominated by a few large extended grains. (right) Mo composition for the same microstructure. The grains solidify with a higher Mo concentration than the liquid, resulting in a lower concentration of Mo in the grain interface region

Fig. 7 Pole figures of the simulated microstructures including the orientations of the 5 RVEs
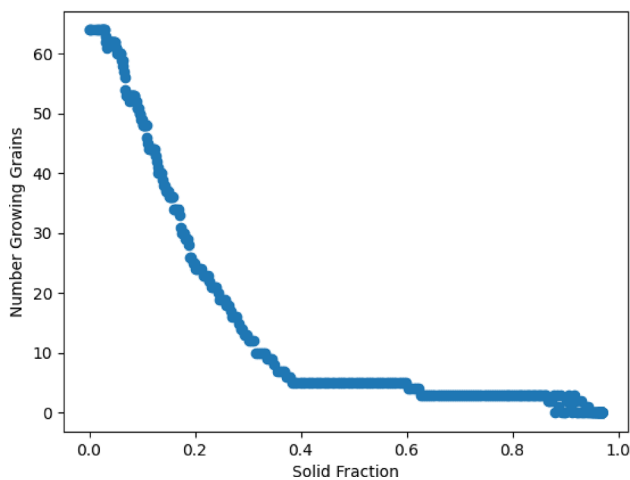
Fig. 8 Number of grains with significant growth, relative to their own current size, as a function of the solid phase fraction. Significant growth is defined as $V_n(t_k) - V_n(t_k - \Delta t)/(V_n(t_k - \Delta t)\Delta t) > 100$. The growth as the solid fraction approach 1 is restricted by the top of the simulation cell

To analyze the growth of the grains, the growth rate of each individual grain was calculated and the number of grains with a significant growth rate was plotted as a function of the fraction of solid in the cell. Figure 8 shows that all but a few grains have stopped having significant growth by the time approximately 40% of the cell have solidified, equivalent to a position of the solidification front of about 24 μm. The remaining grains continue to grow and will become large elongated grains stretching most or all of the cells vertical direction. As these grains are likely to have a favorable orientation relative to the always vertical thermal gradient, they are also likely to continue to grow epitaxially through consecutive layers, provided they connect with the melt pool of the next layer, and form the large elongated grains seen for some combinations of laser power or powder feed rate [21]. Predicting if epitaxial growth will happen is complicated since it depends on heterogeneous nucleation, which phase field models do not predict intrinsically. Nonetheless, the obtained RVEs already show a long textured columnar region, so they should still show mechanical anisotropy and can be used to infer which direction will be stronger in a qualitative sense.

Micromechanical FEA Model

Figure 9 shows the Von mises stress field output of the microstructure loaded in the solidification direction, together with the calculated volume averaged stress–strain curves in different loading directions. The plotted stress–strain curve is an average of the results for 5 different RVEs because the randomness in nucleation can produce significant variations for the small regions modeled. Since the thermal gradients in the melt pool boundary have been shown to be almost vertical in the thermal FEA model, the solidification direction can be assumed to be the vertical Building Direction (BD). This allows to compare the stress–strain of the vertical BD to the two orthogonal horizontal directions. The stress–strain curves correctly show elastic and yield strength isotropic behavior in these directions, which is supported by the experiments in references [21, 22]; meaning that not much difference is expected between loading 3D printed Ti-5553 in the vertical BD or horizontally. This gives freedom to the manufacturer to choose a build orientation that reduces residual stresses or build costs since the material will behave similarly in the two directions. This isotropic behavior is due to the < 100 > fiber texture in the building direction produced by the high vertical thermal gradients on cubic crystals. For BCC crystals, as in Ti-5553, this texture produces similar schmid factors for loading a sample horizontally or vertically [22]. The crystal plasticity model intrinsically accounts for this effect, and is able to predict texture-induced effects on the microstructure's yield strength. Nonetheless, it must be noted that other sources of anisotropy may occur in PBF alloys that the current approach does not account for, like heterogeneous dislocation densities [22] or directionally
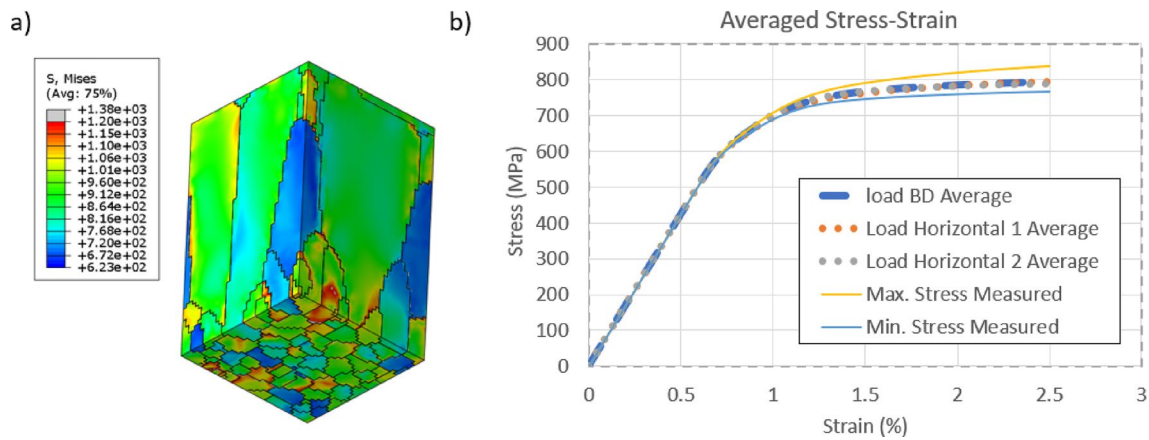
Fig. 9 **a** micromechanics field output of the Von Mises stress of a microstructure loaded in the vertical BD direction. **b** Volume averaged stress–strain curve when the miscrostructure is loaded in different orthogonal directions. The averaged curve corresponds to the average results of 5 RVEs. The maximum and minimum stress curves measured are also shown to give an estimate of the scatter in the results

oriented defects and crack propagation [21], which would require a more advanced constitutive model and microstructure evolution simulation approach to be predicted. These effects will mainly affect hardening behavior, which has been shown to be anisotropic and has not been predicted by this model [21, 22].

Discussion

These results show that it is possible to combine a thermal FEA model of an AM process, a microstructure evolution model in the form of a phase field model and a micromechanics CPFEA model to study the effect of process parameters on homogenized mechanical tensile properties of meta-stable β titanium alloys. The developed process–structure–property model has shown that this material has the same strength in the building and horizontal directions, which can guide manufacturers to choose build orientations freely. Nonetheless, micromechanical CPFEA simulations have also been proven to predict fatigue initiation [23], creep [24], residual stresses [25], tension-compression asymmetry [23] and crack propagation [26], among others. Besides property predictions, they have also been used in plenty of theoretical studies to understand the micromechanical behavior of metals. Therefore, the developed RVE generation and loading approach could also be used to study much more than what has been presented here. Furthermore, since this report has shown that it is straightforward to generate RVEs and load them as desired using widely known commercial tools, we hope to have encouraged the development and use of process–structure–property models for metal manufacturing processes.

Nonetheless, it must be noted that the developed model still required a lot of information from experiments in terms of property inputs for the different simulations as well as for making several modeling choices. The thermal FEA model requires temperature dependent material properties and a laser absorption coefficient. The phase field model needs a phase diagram, and certain assumptions and modeling choices were made were made by looking at metallographic images of the solidified material. Finally, the crystal plasticity model parameters are usually obtained by calibrating them against a tensile test of the material to simulate. This makes the simulation approach developed complicated for novel alloys for which not much experimental information can be found in the literature, which are the ones that would benefit the most from this approach. It also pretty much makes it impossible to use for digital alloy development. For these purposes, the model would need to be coupled with an experimental framework or with other simulation approaches that can yield the needed properties. First principles approaches, together with the CALPHAD method, may be the key to produce a fully digital PSPP approach to alloy development since they have been shown to yield some of the properties needed for these models, and will be studied in future work. Furthermore, the experimental results in terms of anisotropy and crystallographic orientation have shown significant scatter from one microstructure to the other. This means that homogenization strategies with this approach will need a statistical strategy and have potential for uncertainty quantification, which will be studied in future work.

Conclusions

In this work, different physics-based simulations from commercial software tools have been combined to assess the anisotropic tensile properties of PBF Ti-5553. The following conclusions can be made:

- A process thermal FEA model in Abaqus allows to study the solidification temperatures experienced by the material along different regions of the printed component. The temperature gradients and cooling rates obtained can be used for microstructure evolution models of solidification.
- A phase field model of solidification in Material Studio that uses the previous temperature history as input can predict the final microstructure's texture and morphology and can yield an RVE for virtual mechanical testing with PBCs.
- A micromechanics FEA model in Abaqus that digitally stresses the previously obtained RVE allows to assess its bulk mechanical properties in different directions.
- The developed model allowed to predict the textured and elongated grains of meta-stable β alloys and the effects this produces on tensile strength. The simulation predicted similar strengths in the vertical and horizontal directions of AM components. The low magnitude of anisotropy could be attributed to the many slip systems of BCC crystals and the $< 100 >$ fiber texture which produces similar schmid factors on both directions.
- It has been shown that easy to use tools exist for developing 3D representations of the microstructure produced by a given manufacturing process and digitally test them to yield mechanical information. This approach could be extended to study more properties and materials than what has been presented here.
- Most of these models require inputs, physical properties or calibrations obtained from experimental methods. In order to develop fully digital PSPP models of novel alloys, different simulation approaches like density functional theory will probably be needed.

Declarations

Conflict of interest On behalf of all authors, the corresponding author states that there is no conflict of interest.

References

1. Jiang W, Guo X, Deng Y (2022) Anisotropic response in mechanical behavior of additively manufactured Al-Mn-Sc alloys by in-situ ebsd tensile tests. Mater Sci Eng A 858:144155. https://doi.org/10.1016/j.msea.2022.144155
2. Zhang Q, Xie J, Gao Z, London T, Griffiths D, Oancea V (2019) A metallurgical phase transformation framework applied to slm additive manufacturing processes. Mater Des 166:107618. https://doi.org/10.1016/j.matdes.2019.107618
3. Yan W, Lian Y, Yu C, Kafka OL, Liu Z, Liu WK, Wagner GJ (2018) An integrated process-structure-property modeling framework for additive manufacturing. Comput Methods Appl Mech Eng 339:184–204. https://doi.org/10.1016/j.cma.2018.05.004
4. Turner JA, Belak J, Barton N, Bement M, Carlson N, Carson R, DeWitt S, Fattebert J-L, Hodge N, Jibben Z, King W, Levine L, Newman C, Plotkowski A, Radhakrishnan B, Reeve ST, Rolchigo M, Sabau A, Slattery S, Stump B (2022) ExaAM: Metal additive manufacturing simulation at the fidelity of the microstructure. Int J High Perform Comput Appl 36(1):13–39. https://doi.org/10.1177/10943420211042558
5. Motaman SAH, Kies F, Köhnen P, Létang M, Lin M, Molotnikov A, Haase C (2020) Optimal design for metal additive manufacturing: an integrated computational materials engineering (ICME) approach. JOM 72(3):1092–1104. https://doi.org/10.1007/s11837-020-04028-4
6. Knapp GL, Coleman J, Rolchigo M, Stoyanov M, Plotkowski A (2023) Calibrating uncertain parameters in melt pool simulations of additive manufacturing. Comput Mater Sci 218:111904. https://doi.org/10.1016/j.commatsci.2022.111904
7. Abaqus User Manual. https://www.3ds.com/support/documentation/. Accessed: 2010-09-30
8. Materials Studio Collection. https://www.3ds.com/products-services/biovia/products/molecular-modeling-simulation/biovia-materials-studio/materials-studio-collection/
9. OpenPhase-Solutions. https://openphase-solutions.com/
10. Steinbach I (2009) Phase-field models in materials science. Modell Simul Mater Sci Eng 17(7):073001. https://doi.org/10.1088/0965-0393/17/7/073001
11. Steinbach I (2013) Why solidification? why phase-field? JOM 65(9):1096. https://doi.org/10.1007/s11837-013-0681-5
12. Materials Studio Collection. https://www.3ds.com/products-services/biovia/products/molecular-modeling-simulation/biovia-materials-studio/
13. Agius D, O'Toole P, Wallbrink C, Sterjovski Z, Wang C-H, Schaffer GB (2021) Integrating phase field and crystal plasticity finite element models for simulations of titanium alloy ti-5553. J Phys: Mater 4(4):044014. https://doi.org/10.1088/2515-7639/ac194f
14. Thermo-Calc. https://thermocalc.com/
15. Peirce D, Asaro RJ, Needleman A (1982) An analysis of nonuniform and localized deformation in ductile single crystals. Acta Metall 30(6):1087–1119. https://doi.org/10.1016/0001-6160(82)90005-0
16. Huang Y (1991) A user-material subroutine incorporating single crystal plasticity in the ABAQUS finite element program. Harvard Univ, Cambridge
17. Pilgar CM, Fernandez AM, Segurado J (2023) Microstructure sensitive fatigue life prediction model for slm fabricated hastelloy-x. Int J Fatigue 168:107372. https://doi.org/10.1016/j.ijfatigue.2022.107372
18. Sedighiani K, Shah V, Traka K, Diehl M, Roters F, Sietsma J, Raabe D (2021) Large-deformation crystal plasticity simulation of microstructure and microtexture evolution through adaptive remeshing. Int J Plast 146:103078. https://doi.org/10.1016/j.ijplas.2021.103078
19. Emdadi A, Asle Zaeem M (2021) Phase-field modeling of crack propagation in polycrystalline materials. Comput Mater Sci 186:110057. https://doi.org/10.1016/j.commatsci.2020.110057
20. Schwab H, Palm F, Kühn U, Eckert J (2016) Microstructure and mechanical properties of the near-beta titanium alloy ti-5553

processed by selective laser melting. Mater Design 105:75–80. https://doi.org/10.1016/j.matdes.2016.04.103

21. Hicks C, Konkova T, Blackwell P (2020) Influence of laser power and powder feed rate on the microstructure evolution of laser metal deposited Ti-5553 on forged substrates. Mater Charact 170:110675. https://doi.org/10.1016/j.matchar.2020.110675

22. Huang H, Zhang T, Chen C, Hosseini SRE, Zhang J, Zhou K (2022) Anisotropy in the tensile properties of a selective laser melted Ti-5Al-5Mo-5V-1Cr-1Fe alloy during aging treatment. Materials (Basel) 15(16):5493. https://doi.org/10.3390/ma151 65493

23. Gopalakrishnan S, Bandyopadhyay R, Sangid MD (2022) A framework to enable microstructure-sensitive location-specific fatigue life analysis of components and connectivity to the product lifecycle. Int J Fatigue 165:107211. https://doi.org/10.1016/j. ijfatigue.2022.107211

24. Li K-S, Wang R-Z, Yuan G-J, Zhu S-P, Zhang X-C, Tu S-T, Miura H (2021) A crystal plasticity-based approach for creep-fatigue life prediction and damage evaluation in a nickel-based superalloy. Int J Fatigue 143:106031. https://doi.org/10.1016/j.ijfatigue.2020. 106031

25. Agaram S, Srinivasan SM, Kanjarla AK (2022) Crystal plasticity modelling of stability of residual stresses induced by shot peening. Int J Mech Sci 230:107526. https://doi.org/10.1016/j.ijmec sci.2022.107526

26. Lucarini S, Dunne FPE, Martínez-Pañeda E (2023) An fft-based crystal plasticity phase-field model for micromechanical fatigue cracking based on the stored energy density. Int J Fatigue 172:107670. https://doi.org/10.1016/j.ijfatigue.2023.107670